RSC Advances

ROYAL SOCIETY OF CHEMISTRY

www.rsc.org/advances

RSC Advances

RSCPublishing

ARTICLE

ZnO Nanopinecone Arrays with Enhanced Photocatalytic Performance in Sunlight

Cite this: DOI: 10.1039/xoxxoooooox

Yu-Cheng Chang*

A novel ZnO nanopinecone was fabricated by a wet chemical approach in an aqueous solution of ascorbic acid. The ZnO nanorods layer facilitated the growth of aligned nanopagodas, stacking nanoplates, and nanopinecones. The correlation between the concentration of zinc precursor (zinc nitrate and HMTA) and L-ascorbic acid was exploited to control the morphologies of ZnO nanostructures for the same reaction conditions. The complex ZnO nanostructures exhibited very strong and sharp ultraviolet emissions from the band gap, while almost no green emission was attributed to singly ionized oxygen vacancies in the cathodoluminescence spectra. ZnO nanopinecones can provide a higher surface-to-volume ratio and better stability against aggregation with more polar surface exposure, resulting in their highest photocatalytic performance in sunlight. The ZnO nanopinecone arrays are beneficial in fabricating novel devices, such as ultraviolet lasers, light-emitting devices, and dye-sensitized solar cells.

Received ooth January 2014,
Accepted ooth January 2014

DOI: 10.1039/xoxxoooooox

www.rsc.org/

Introduction

Zinc oxide (ZnO) has been recognized as one of the most important semiconductor materials for optoelectronics and piezoelectricity effects because of its wide direct band-gap (3.37 eV), large exciton binding energy (60 meV), and non-centrosymmetric structure.[1-3] The high exciton binding energy in ZnO crystals can ensure efficient excitonic emissions at room temperature.[4] ZnO is transparent in visible light and can be made highly conductive by doping.[5] Furthermore, ZnO is bio-safe and biocompatible, and it can be directly used for biomedical applications without coating.[3, 6, 7] ZnO is also versatile and has promising applications in nanodevices such as ultraviolet (UV) lasers,[8, 9] light-emitting diodes (LED),[10, 11] photonic crystals,[12, 13] chemical sensors,[14, 15] field emission transistors (FET),[16-18] piezoelectric nanogeneators,[19-21] and solar cells.[22, 23]

ZnO nanostructures have been fabricated through various techniques, such as chemical vapor deposition (CVD),[24] metal-organic chemical vapor deposition (MOCVD),[25, 26] physical vapor deposition (PVD),[4, 27] molecular beam epitaxy (MBE),[28] pulsed laser deposition,[29, 30] thermal evaporation,[6, 31] and wet chemical methods.[32-34] Among them, wet chemical method is some of the most attractive technique because it is low cost, low temperature, less hazardous, compatible with flexible organic substrates, and thus capable of easy scaling up.[33] In addition, wet chemical method has been demonstrated as very powerful and versatile technique for growing ZnO nanostructures.[32] Recently, there have been extensive reports on the fabrication of different ZnO nanostructures by a wet chemical method, such as nanorods,[13, 35] nanowires,[33, 36] nanotubes,[37] nanoflowers,[38, 39] nanoribbons,[40] nanoneedles,[41] nanotowers,[42] nanosheets,[43] and nanoplates.[44]

Previous works of wet chemical processes focused on controlling the reaction time, solution concentration, and different pH values and reagents to produce ZnO nanostructures with different morphology.[33, 45] Wang et al. obtained the submicron tower-like, flower-like, and tube-like ZnO crystal arrays in a reaction solution system that included zinc nitrate, ammonia, ammonium salt, and thiourea.[46] ZnO nanotower bundles have been grown on electrochemically deposited ZnO thin films by a hydrothermal process. The reaction in a solution of zinc nitrate and hexamethylenetetramine (HMTA) occurred at 90 °C for 3h.[42] Tian et al. demonstrated that the reaction solution of zinc nitrate and HMTA, with the addition of sufficient sodium citrate, would change the morphology from nanorods to nanoplates with a long reaction time. The citrate ions that participated in the reaction would make the structures relatively complex.[34, 47, 48] As new methodologies and strategies to guide the design and solution synthesis of new morphologies have developed, capping reagents have been successfully used to control the sizes and shapes of ZnO nanostructures.[32, 34, 49] The capping reagents have a remarkable ability to control the shapes of ZnO nanostructures. However, many reagents pollute the environment and are detrimental to human health.

The ability to adopt non-toxic and bio-friendly reagents for controlling and integrating nanostructures as functional 3-D arrays is an important challenge for scientists have faced to develop biotechnology and environment.[50, 51] In our previous work, L-ascorbic acid (ascorbic acid for simplicity), which is free from health hazards, had been used to control the morphology of ZnO nanostructures.[50] L-ascorbic acid—a form of ascorbic acid, and also called Vitamin C—is a water-soluble nutrient that is essential for maintaining human health.[52] The present study uses an appropriate

concentration of precursor (zinc nitrate, HMTA, and ascorbic acid) in conjunction with a wet chemical process to produce various ZnO nanostructures in a short time. The ZnO nanorods layer plays a crucial role in determining the alignment of ZnO nanostructures. The ZnO nanostructures exhibit a very prominent blue shift in UV emissions and almost no green emissions attributed to singly ionized oxygen vacancies. The enhancement in deep-UV emissions shall be advantageous in applications for nanoscale light-emitting devices. The novel structured ZnO nanopinecones have shown a structure-induced enhancement of photocatalytic performance by higher surface-to-volume ratio and a more exposed polar surface, which exhibits a much better photocatalytic property for the photodegradation of phenol in sunlight. The novel ZnO nanostructures are expected to have excellent potential for surface-related applications.

Experimental

Synthesis

A Si (001) wafer was cleaned ultrasonically for 10 min in ethanol. A thin film of zinc acetate was then coated on the substrate by spinning a layer of 5 mM zinc acetate dihydrate (98%, Aldrich) in ethanol; this process was repeated ten times. 5-10 nm thick ZnO seeds film was produced after annealing at 300 °C in air for 20 min.[41] The ZnO nanorods layer was grown by a wet chemical method in 100 mL of aqueous solution containing 50 mM zinc nitrate hexahydrate (98%, Aldrich) and hexamethylenetetramine (99%, Aldrich) (HMTA). The substrate with nanorods was placed downward near the surface of the reaction solution and heated to about T = 90 °C for 3hr.[50] The ZnO nanostructures were grown by wet chemical and downward growth methods in a 100 mL aqueous solution. The solutions contained various equimolar zinc nitrate hexahydrate and HMTA with the addition of different concentration of ascorbic acid (99 %, Aldrich). The reaction proceeded at T = 90 °C for 3hr. The substrate film was either a ZnO seeds layer or a ZnO nanorods layer.

Characterization

The morphology of nanostructures was examined with a field emission scanning electron microscope (FESEM) using a JEOL JSM-6500F SEM operating at 10 kV accelerating voltage. A JEOL-2010 transmission electron microscope (TEM) operating at 200 kV was used to examine the microstructures. The crystalline phase of the ZnO nanostructures was determined using the X-ray powder diffraction method (Shimadzu XRD-6000, CuKα1 radiation (λ = 0.1505 nm)). The cathodoluminescence (CL) spectra were acquired with an electron probe microanalyzer (Shimadzu EPMA-1500) attached to a SEM. CL spectra were accumulated in a single shot mode within an exposure rate of 1 nm/s. All the CL spectra were taken at room temperature. For the photocatalytic activity evaluation, the concentration of photodegraded phenol was recorded by a Hitachi U-2900 UV-vis spectroscopy.

Results and Discussion

In our previous work, the alignment of ZnO nanorods was found to increase with the number of times spin-coated ZnO seeds were layered—up to ten times. For spin coating above ten times, the sizes of the ZnO nanorods became rather non-uniform.[41] Heating during the deposition was found to produce ZnO seeds with [001] planes parallel to the substrate surface.[53] The aligned ZnO seeds were examined with transmission electron microscopy (TEM) to understand their microstructure and mechanism of formation. Figure 1a shows a TEM image of ZnO seeds with diameter of 5-10 nm. The polycrystalline diffraction pattern (not shown) lacks the (002) ring, as expected for seeds with strong c-axis texturing normal to the membrane and no in-plane rotational alignment. Figure 1b shows a SEM image depicting the ZnO nanopagodas grown from an equimolar (5 mM) zinc nitrate and HMTA reaction solution with small amount of ascorbic acid (0.1875 mM) by a wet chemical and downward growth process. The substrate was covered with ZnO seeds layer (Fig. 1a) prepared with a total growth time of 3h. The growth direction of ZnO nanopagodas exhibited random orientation, and the macroscopic structure was similar to the bundle-like arrangement found on the seeds layer. Although the ZnO seeds layer has been extensively investigated to grow the vertically aligned ZnO nanorods,[13] nanowires,[53] and nanoneedles,[41] this strategy has not been used for the preparation and systematic control of large arrays of oriented nanopagodas.

In order to improve the alignment of nanopagodas, vertically aligned ZnO nanorod arrays were used as seed growth. The vertical alignment and smooth top surface of ZnO nanorod arrays were grown from equimolar (50 mM) zinc nitrate and HMTA for 3h by the downward growth method, as shown in Figure 1c. The diameters and lengths of the nanorods are 35-95 nm and 1.5-2.1 μm, respectively. The ZnO nanorod arrays can provide better surface coverage and enhance the growth of more uniform ZnO nanopagoda arrays on the silicon wafer. Figure 1d shows a top-view SEM image depicting laminated ZnO nanopagoda arrays grown with equimolar (5 mM) zinc acetate and HMTA, as well as 0.1875 mM ascorbic acid on the ZnO nanorods layer by the downward growth method. The tip diameters and lengths of nanopagodas are 3-17 nm and 1.3-1.8 μm, respectively. The ZnO nanorods layer can be effectively used to grow aligned ZnO nanopagoda arrays. The oriented nanorod arrays shall be beneficial for growing other complex ZnO nanostructures with controlled crystalline morphology.

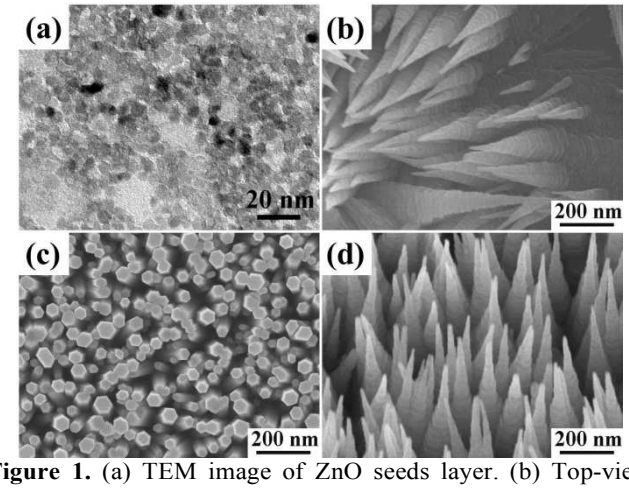

Figure 1. (a) TEM image of ZnO seeds layer. (b) Top-view SEM image of ZnO nanopagodas grown on Si wafer with ZnO seeds layer. (c) Top-view SEM image of ZnO nanorod arrays grown on Si wafer with ZnO seeds layer. (d) 20° tilt-view SEM image of ZnO nanopagoda arrays grown on Si wafer with ZnO nanorods layer.

The variation in the concentration of zinc precursor (zinc nitrate and HMTA) and ascorbic acid was found to affect the

apex angles of the nanopagodas.[50] The present work investigates the influence of low and high precursor concentration. Figure 2a shows a 20° tilt SEM image depicting the ZnO nanopagodas with rod-like structures. The tip diameters and lengths of the rod-like nanopagodas are 7-29 nm and 1.2-1.7 μm, respectively. The rod-like ZnO nanopagodas were grown from equimolar (2.5 mM) zinc nitrate, HMTA, and low concentration of ascorbic acid (0.09375 mM) reaction solution. Figure 2b shows a 20° tilt SEM image depicting the ZnO nanopagodas with hexagonal pyramid-like structures. The tip diameters and lengths of pyramid-like nanopagodas are 5-24 nm and 560-790 nm, respectively. The pyramid-like ZnO nanopagodas were grown from equimolar (10 mM) zinc nitrate, HMTA, and (0.375 mM) ascorbic acid reaction solution. The heights of the pyramid-like ZnO nanopagodas were found to decrease relative to the lower concentration of ascorbic acid. When the concentration of the equimolar (20 mM) zinc nitrate, HMTA, and (0.75 mM) ascorbic acid reaction solution was increased, the pyramid-like ZnO nanopagoda arrays increased in sizes and almost bound together, as shown in Fig. 2c. Figure 2d shows a 20° tilt SEM image of ZnO nanostructures prepared with equimolar (40 mM) zinc nitrate, HMTA, and (1.5 mM) ascorbic acid reaction solution. The morphology of ZnO nanostructures is similar to stacking nanoplate arrays. The surface of stacking nanoplate is relatively rough and irregular. The variation in precursor concentration is useful in controlling the growth of different morphology of ZnO nanostructures.

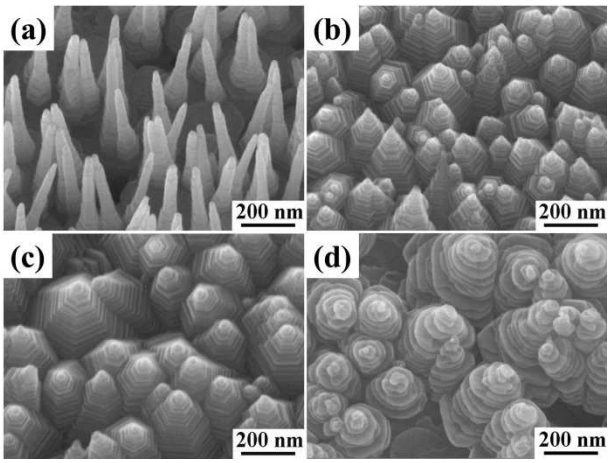

Figure 2. 20° tilt-view SEM images of (a-c) ZnO nanopagoda arrays and (d) ZnO stacking nanoplate arrays grown on Si wafer with ZnO nanorods layer. The concentration of equimolar zinc nitrate, HMTA, and ascorbic acid are (a) 2.5 mM (0.09375 mM), (b) 10 mM (0.375 mM), (c) 20 mM (0.75 mM) and (d) 40 mM (1.5 mM), respectively.

Figure 3 shows the XRD patterns of the substrates fabricated with different ZnO nanostructures. The XRD pattern of the ZnO nanorods layer is shown in Fig. 3a. A strong and sharp diffraction peak corresponding to the [002] crystal plane of ZnO indicates that the preferred growth direction of the ZnO nanorods layer is in the [001] direction. Figure 3b shows the XRD pattern of rod-like and pyramid-like ZnO nanopagoda arrays grown with equimolar (2.5 or 10 mM) zinc nitrate, HMTA, and (0.09375 or 0.375 mM) ascorbic acid reaction solutions, respectively. The XRD pattern is also the same (Fig. 3a) with the only growth direction [002]. When the concentration equimolar (20 mM) zinc nitrate, HMTA and (0.75 mM) ascorbic acid reaction solution was increased, the XRD pattern displayed three peaks, as shown in Figure 3c. The three peaks are [100], [002], and [101], respectively. The peak [002] is showing greater strength than the other peaks. The results indicate that the large sizes of ZnO pyramid-like nanopagodas (Fig. 2c) still represent the normal c-axis preferential orientation. Figure 3d shows the XRD pattern of ZnO stacking nanoplate arrays (Fig. 2d). Compared to the XRD peaks, the intensity of [002] is only twice that of [100]. The zinc precursor (zinc nitrate and HMTA) and ascorbic acid could greatly change the ZnO preferential growth orientation.

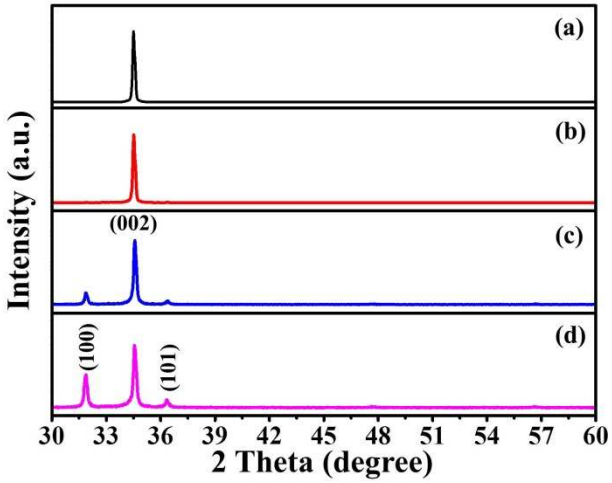

Figure 3. XRD spectra of (a-c) ZnO nanopagoda arrays and (d) ZnO stacking nanoplate arrays grown on Si wafer with ZnO nanorods layer. The concentration of equimolar zinc nitrate, HMTA and ascorbic acid are (a) none, (b) 2.5 or 10 mM (0.09375 or 0.375 mM), (c) 20 mM (0.75 mM) and (d) 40 mM (1.5 mM), respectively.

The enormous change in the ZnO nanostructures can be attributed to the concentration of zinc precursor (zinc nitrate and HTMA) and ascorbic acid. Previous work has shown that ZnO nanowires with diameters of 10-20 nm and 100-200 nm were grown in 1 and 10 mM zinc precursor solutions, respectively.[36, 54] The sizes of the ZnO nanowires could be controlled by changing the zinc precursor within the same reaction conditions. One-dimensional ZnO nanostructures are easily grown along the c axis of the Wurtzite crystal, which has a hexagonal structure with six nonpolar {10-1} prisms capped by polar oxygen [00-1] and zinc [001] basal surfaces.[6] The polar surface of the [001] plane can be terminated with the top surfaces of positively charged [001]-Zn and the bottom surfaces of negatively charged [00-1]-O, respectively.[32] The chemical structures of ascorbic acid have two hydroxyls (O-H) and one carbon-oxygen double bond (C=O). The lone pairs of electrons can bind to the positively charged [001]-Zn polar plane and slow down crystal growth along the [001] direction by electrostatic force.[50] These phenomena are similar to citrate ions that can strongly and specifically adsorb to the positively charged [001]-Zn polar plane, and thus inhibit the growth along [001].[34] The electrostatic interaction and distinct chemical activities of the polar surfaces are conductive to the formation of nanoplates. Herein, the concentration of zinc precursor (zinc nitrate and HTMA) and ascorbic acid are important for controlling the morphology from nanopagodas to nanoplates.

Figure 4a shows a TEM image of a rod-like ZnO nanopagoda (in Fig. 2a) with a length of 977 nm and a tip diameter of about 18 nm. The rod-like ZnO nanopagoda is very narrow and long

and has a small angle of 3° in the extended line. The high-resolution TEM image taken from part of an individual rod-like nanopagoda and the corresponding selected area electron diffraction (SAED) pattern are shown in Figs. 4b and c, respectively, and displays a (010) zone-axis SAED pattern. Both the TEM image and diffraction pattern indicate that the rod-like nanopagoda is single-crystalline and grown in [001] direction. Figure 4d shows a TEM image of a pyramid-like ZnO nanopagoda (in Fig 2c) with a length of 328 nm and tip diameter of about 8 nm. The pyramid-like ZnO nanopagoda has an angle of 14°. The high-resolution TEM image taken from part of an individual pyramid-like ZnO nanopagoda and the corresponding SAED pattern is shown Figs. 4e and f, respectively, which also shows the same (010) zone-axis SAED pattern. Both the TEM image and diffraction pattern indicate that the pyramid-like ZnO nanopagoda is also single-crystalline and grown in [001] direction. The above results clearly reveal that the angles and concentrations of zinc precursor have the same tendency. Accompany with the increase in the concentration of zinc precursor (zinc nitrate and HMTA) and ascorbic acid, the laminated structures become more evident.

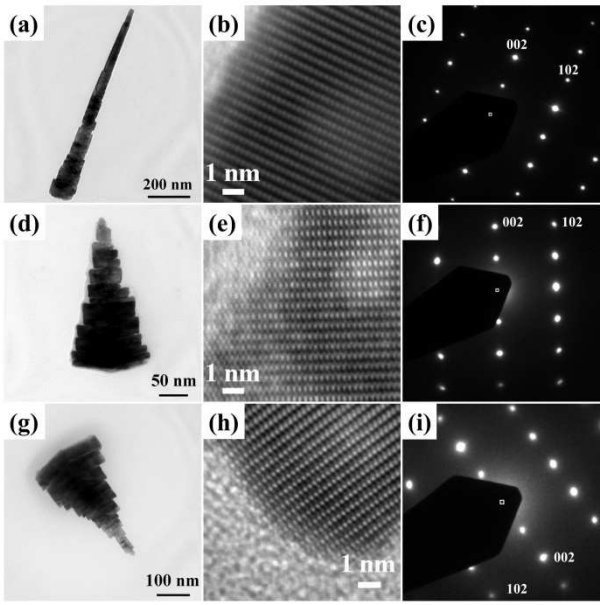

Figure 4. (a) TEM image of a rod-like nanopagoda in Fig. 2a. (b) HRTEM and (c) SAED pattern confirming the single-crystallinity of the rod-like nanopagoda in (a). (d) TEM image of a pyramid-like nanopagoda in Fig. 2b. (e) HRTEM and (f) SAED pattern confirming the single-crystallinity of the pyramid-like nanopagoda in (d). (g) TEM image of a stacking nanoplate in Fig. 2d. (h) HRTEM and (i) SAED pattern confirming the single-crystallinity of the stacking nanoplate in (g).

With increasing in the concentration of equimolar (40 mM) zinc nitrate, HMTA and (1.5 mM) ascorbic acid reaction solutions, the morphology of ZnO stacking nanoplate arrays is evident the different from nanopagodas. Figure 4g shows a TEM image of a ZnO stacking nanoplate with a length of 389 nm and tip diameter of about 10 nm. The high-resolution TEM image taken from part of an individual ZnO stacking nanoplate and the corresponding SAED pattern are shown Figs. 4h and i, respectively. The image also shows the same (010) zone-axis SAED pattern. Both the TEM image and diffraction pattern indicate that the ZnO stacking nanoplate is still single-crystalline and grown in [001] direction. Although ascorbic acid has inhibited ZnO nanostructures to grow along [001], the HRTEM image and SAED pattern exhibit that the plane of [001] is major grow direction. The results show that 1.5 mM of ascorbic acid cannot completely influence the growth along the high activity of [001] plane.

To understand the different concentration of ascorbic acid shall be impacted ZnO nanostructures at the high concentration of zinc precursor. The concentration-dependent morphological evolution process was examined by FESEM. Figure 5 shows the morphology of the ZnO nanostructures grown in different concentration of ascorbic acid with 40 mM zinc precursor. With the addition of ascorbic acid (1.2 mM), screw-like ZnO nanostructures were formed and exhibited the random orientation from the substrate, as shown in Fig. 5. The morphology of screw-like ZnO nanostructures is relatively different from ZnO stacking nanoplates (1.5 mM ascorbic acid). The ZnO nanostructures are appreciably changed by the slight variation in the concentration of ascorbic acid. As the concentration of ascorbic acid is increased to 1.8 mM, the laminated and tapered ZnO nanostructures, herein call nanopinecones, are formed, as shown in Fig. 5b. The ZnO nanopinecones are not only distinct from stacking nanoplates, but they are also relatively complicated for nanopagodas. The growth of ZnO nanopinecone is correlated with the downward growth process and attributed to the gradual depletion of precursor in the solution during growth. Figure 5c and d show the SEM images of samples prepared with the addition of 2.0 and 2.2 mM ascorbic acid, respectively. The morphology exhibits the complete ZnO nanoplate structure, which is similar to a mica sheet. The thicknesses of ZnO nanoplates are significantly decreased with the increase in concentration of ascorbic acid. The varied concentrations of ascorbic acid are useful in controlling grow the different morphologies of ZnO nanostructures, such as screw-like nanostructures, stacking nanoplates, nanopinecones, and nanoplates.

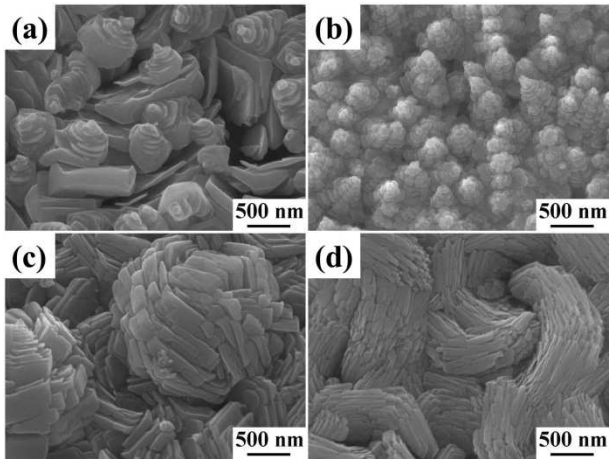

Figure 5. 20° tilt-view SEM images of ZnO nanostructures grown on Si wafer with ZnO nanorods layer at the concentration of 40 mM zinc precursor and variable ascorbic acid. The concentrations of ascorbic acid are (a) 1.2 mM, (b) 1.8 mM, (c) 2.0 mM and (d) 2.2 mM, respectively.

Figure 6a shows a top-view high magnification SEM image of a nanopinecone grown with 1.8 mM ascorbic acid and 40 mM zinc precursor. ZnO nanopinecone clearly exhibits a layered and coned structure. Figure 6b shows a TEM image of a ZnO nanopinecone with a length of 358 nm and tip diameter of

about 61 nm. The high-resolution TEM image taken from part of an individual ZnO nanopinecone and the corresponding SAED pattern are shown in Fig. 6c and the inset, respectively. It shows the same (010) zone-axis SAED pattern. Both the TEM image and diffraction pattern indicate that the ZnO nanopinecone is single-crystalline and grown in [001] direction. The nanopinecone structure is similar to the nanopagoda with anisotropic etchings at their corners. In our previous work, the hexagonal nanopagoda shows a single-crystal structure, with [001] top/[00-1]bottom surfaces and [1-10] side surfaces.[50] From the crystal structure, ZnO can be described as a number of alternating planes composed of tetrahedrally coordinated O^{2-} and Zn^{2+} ions, stacked alternately along the c axis. The corner anisotropic etchings on the surface of the nanopinecones may be due to the dependence of the local etching rate on the crystal orientation. On the other hand, the etching rate could also be sensitive to the concentration of ascorbic acid.

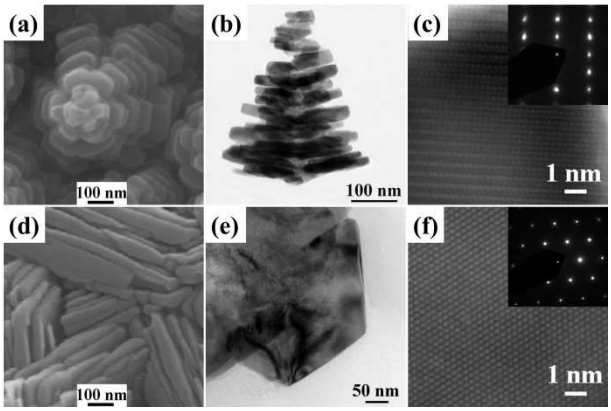

Figure 6. (a) 20° tilt-view high magnification SEM image of ZnO nanopinecones grown on Si wafer with ZnO nanorods layer. (b) TEM image of a nanopinecone in (a). (c) HRTEM image and SAED pattern confirming the single-crystallinity of the nanopinecone in (b). (d) 20° tilt-view high magnification SEM image of ZnO nanoplates grown on Si wafer with ZnO nanorods layer. (e) TEM image of a nanoplate in (d). (f) HRTEM image and SAED pattern confirming the single-crystallinity of the nanoplate in (e).

The oriented nanorod arrays are beneficial for growing ZnO nanostructure arrays with morphologies of nanoplates, nanopagodas, and nanopinecones. When ZnO nanorod arrays were changed to ZnO seeds layer, the morphologies of the ZnO nanostructures appeared non-uniform and discontinuous. Figure 1S shows the SEM images of ball-like ZnO nanoplates grown in 2.2 mM of ascorbic acid with 40 mM zinc precursor. The unfavorable self-seeded growth is attributed to difficulty in nucleation on the ZnO seeds layer, which was exacerbated by a downward gravitational pull of the reagents. On the other hand, the ZnO nanorods layer can be effectively used to grow aligned ZnO nanostructures. Figure 6d shows a top-view high magnification SEM image of nanoplates grown with 2.2 mM ascorbic acid and 40 mM zinc precursor on a ZnO nanorods layer (Fig. 5d), which displays a layered and stacked nanoplate structure. Figure 6e shows a TEM image of the side of a ZnO nanoplate. The high-resolution TEM image taken from part of an individual ZnO nanoplate and the corresponding SAED pattern is shown in Fig. 6f and inset, respectively. It shows the (001) zone-axis SAED pattern. Both the TEM image and diffraction pattern indicate that the ZnO nanoplate is also single-crystalline and grown in [001] direction.

Cathodoluminescence (CL) is a beneficial technique for characterizing the optical properties of nanostructures. Since CL uses an electron beam for excitation, it is feasible to excite only a single or a small group of nanostructures. All the CL spectra were taken at room temperature.[13, 41] The CL spectrum of ZnO nanorod arrays (Fig. 1c) were grown on the ZnO-coated Si substrate, as shown in Fig. 7a. The weak UV emission is at about 381 nm (3.25 eV), which comes from a recombination of excitons and a very strong green emission at about 562 nm. This result is consistent with the currently accepted model that the green emission arises from the recombination between holes trapped at the surface defect and electrons trapped at the oxygen vacancy.[41] Figure 7b represents screw-like ZnO nanostructures grown with 40 mM zinc precursor and 1.2 mM of ascorbic acid ((Figure 5a)) on a ZnO nanorods layer. For the screw-like ZnO nanostructures, strong UV emission occurs at about 374 nm (3.32 eV), which comes from a recombination of excitons and almost no emission form defects. The blue shift is attributed to the quantum confinement effect arising from the reduced sizes of each plate. In the CL emission spectra, the energy shift of nanorods with diameters far beyond the quantum confinement regime is ascribed to the surface effect due to the increased surface-to-volume ratio.[55] For ZnO stacking nanoplate arrays with 40 mM zinc precursor and 1.5 mM of ascorbic acid (Figure 2d), a strong UV emission is at 375 nm (3.31 eV) and no defect emission, as shown in Fig. 7c. The ZnO stacking nanoplate arrays are stacked with very thin nanoplates, which also exhibit a quantum confinement effect and lead to a blue shift of UV emission. From the above results, the growth processes of ZnO nanostructures with zinc precursor and ascorbic acid can be used to repair the surface defect from a ZnO nanorods layer. The optical properties demonstrate that ascorbic acid is a practical reagent to prepare ZnO nanostructures with superb UV emission and almost no green emission properties.

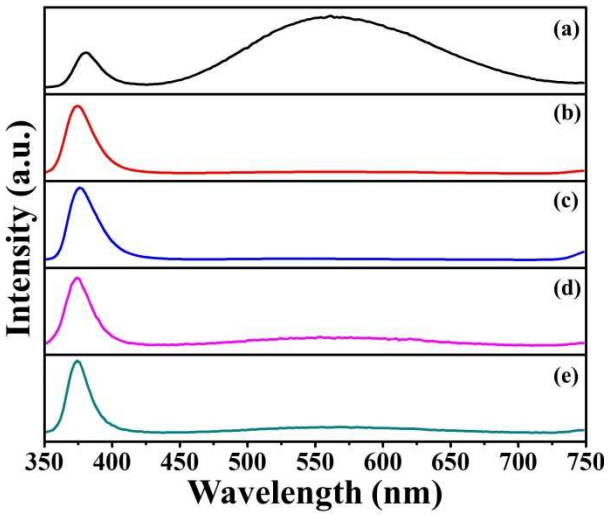

Figure 7. Cathodoluminescence spectra of ZnO nanostructures grow on Si wafer with ZnO nanorods layer. (a) none (only nanorods layer), (b) nanopagodas (c) stacking nanoplates, (d) nanopinecones, and (e) nanoplates.

Figure 7d shows the CL spectrum of ZnO nanopinecones with 40 mM zinc precursor and 1.8 mM of ascorbic acid (Fig. 5b) grown on a ZnO nanorods layer. The ZnO nanopinecones exhibit a sharp UV emission at 374 nm (3.32 eV) and very weak green emission from defect at 554 nm. Compared with

ZnO nanorods layer, green emission was diminished and UV emission became sharper and stronger. The ZnO nanopinecones are constructed by the ZnO nanoplates with very thin (5-30 nm) and uniform thicknesses, which can induce sharp UV emission. For the ZnO nanoplates with 40 mM zinc precursor and 2.2 mM of ascorbic acid, a sharp UV emission at 374 nm and very weak defect emission at 554 nm was observed, as shown in Fig. 7e. Both nanopinecones and nanoplates reveal the similar optical properties with sharp UV emission and weak green emission from defect. Although zinc precursor and ascorbic acid can be used to repair the surface defect from a ZnO nanorods layer, the excessive ascorbic acid can be shown to etch the ZnO nanostructures with surface defects. The etch effect of excessive ascorbic acid is similar to the high concentrations of citrate ions can also cause ZnO nanostructures to become rough and porous during the growth process.[56] The only enhancement in deep-UV optical properties shall facilitate the applications of nanostructures for nanoscale light-emitting or ultraviolet laser devices.

ZnO has been extensively used as a photocatalyst to degrade environmental pollutants, because of its nontoxic nature, low cost, and high photochemical reactivity.[56-58] ZnO nanostructures are efficient photocatalysts due to their high surface-to-volume ratio in comparison with ZnO bulk materials.[56-58] Generally, the photocatalytic activity of powders toward the photodegradation of dyes is applied by using a UV lamp as a light source and the solution under continuous stir.[59] Furthermore, the dispersion in the solution for the recovery of zinc oxide powders is difficult and can easily result in environmental pollution. Herein, ZnO nanostructures grown on a 1 cm × 1 cm Si substrate were used as samples to degrade phenol in sunlight. The schematic method and substrates were used to catalyze the degradation of phenol by sunlight, as shown in Fig. 2S. The substrate was positioned at the bottom of the glass bottle with no stirring. This photocatalytic process was allowed to proceed for 120 min at room temperature.

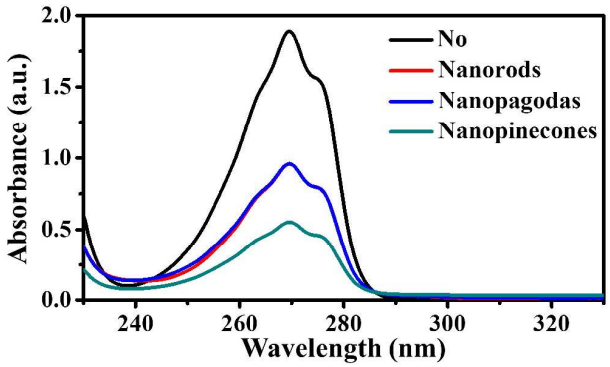

Figure 8. UV-vis absorption spectra of phenol solution illumined under sunlight for 120 min on a silicon substrate with the different ZnO nanostructures.

Figure 8 shows the UV-vis absorption spectra of 1 mM phenol solution illumined under sunlight for 120 min on a silicon substrate with different ZnO nanostructures, including nanorods, nanopagodas, and nanopinecones as well as one sample with no ZnO nanostructure at all. Under the same conditions, the ZnO nanopinecones have much greater photocatalytic activity in the decomposition of phenol compared to nanorods or nanopagodas. The ZnO nanopinecones exhibit high surface-to-volume ratios and stability against aggregation, resulting in the highest photocatalytic efficiency. Cao et al. have reported that ZnO stacked nanoplate arrays with dominated polar surfaces (c plates) exhibit higher photocatalytic efficiency in the decomposition of methylene blue than that of nanowire arrays.[56] ZnO nanopinecones have also been shown to provide large exposures of c plates, which can easily absorb and decompose phenol on the enlarged surface. In general, ZnO nanopagoda arrays grown on ZnO nanorod arrays can provide a greater surface-to-volume ratio and a more exposed polar surface to induce better photocatalytic efficiency. However, the ZnO nanorod and nanopagoda arrays obtained similar photocatalytic efficiencies, the results are attributed to a decrease in the surface-to-volume ratio of nanopagoda arrays. The surface and interval of ZnO nanorod arrays was completely covered with ZnO nanoplates during the growth process of ZnO nanopagoda arrays. Furthermore, the densities of ZnO nanopagodas were lower than nanorods. These two effects make nanopagodas and nanorods with similar photocatalytic efficiencies.

In general, ZnO intrinsic defects, such as oxygen vacancies, can serve electron acceptors and trap the photoinduced electrons temporarily to restrain the undesirable recombination.[60] Therefore, the largest amount of intrinsic defects also plays a vital role in the predominant photodegradation efficiency. Compared to CL results, ZnO nanorods can provide high concentration of oxygen vacancies and surface defects to enhance the photocatalytic efficiency. Herein, the photocatalytic efficiency of nanorods was lower than nanopinecones owing to the photocatalytic process under no stirring and less polar surfaces. The photocatalytic process under no stirring tends to decrease the reaction of phenol and nanorods. The phenomenon is attributed to the phenol molecular being unable to react with the high density and low interval of nanorods. In addition, the polar surfaces can expedite the reaction of phenol and ZnO nanostructures. ZnO nanopinecones can provide better geometry and higher polar surfaces to enhance the photocatalytic efficiency.

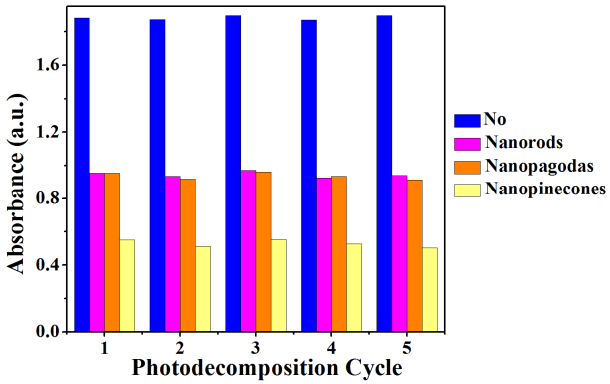

Figure 9. The maximum absorption intensity at 269.5 nm as function of photodecomposition cycles for the different ZnO nanostructures.

For the successful exhibition of these nanostructures as effective photocatalysts, we used recyclable photocatalysts for further studying. The phenol solutions with the different ZnO nanostructures on silicon substrates illumined under sunlight for 120 min, the substrates were rinsed with de-ionized water to remove the residual phenol and dried under a N_2 purge. The substrates were immersed into fresh phenol solution with the same concentrations for another cycle of photodecomposition experiment. The results demonstrate that ZnO nanostructures

can serve as highly effective and convenient recyclable photocatalysts, as shown in Fig. 9. After five cycles, nanopinecones maintain the highest photocatalytic activity rather nanorods and nanopagodas. SEM examination of the substrates after five cycles suggested that the nanopinecones appearance and density did not show evidence change. Hence, ZnO nanopinecones are expected to have a long service lift as photocatalysts with high efficiency and durability. Moreover, ZnO nanopinecones are grown on a silicon substrate, which simplify the recycling process, making ZnO nanostructures steady and economical photocatalysts.

Conclusions

Aligned ZnO nanopinecones have been synthesized on the previously grown and aligned ZnO nanorods on Si wafer using a facile wet chemical method. The substrate with ZnO nanorods layer was found to be critical in obtaining the desired ZnO nanostructures with better orientation and density. The complex ZnO nanostructures were presented for controlling the morphology by experimental conditions, such as the concentration of the zinc precursor and ascorbic acid. The ZnO nanostructures exhibited a significantly strong and sharp UV emission with almost no green emission, which was attributed to singly ionized oxygen vacancies. ZnO nanopinecones have shown a structure-induced enhancement of photocatalytic performance by higher surface-to-volume ratio and a more exposed polar surface, which exhibited a much better photocatalytic property for the photodegradation of phenol in sunlight. The ZnO nanopinecone arrays shall be beneficial in fabricating novel devices, such as ultraviolet lasers, light-emitting devices, and dye-sensitized solar cells.

Acknowledgements

This study was supported financially by the National Science Council, Taiwan (NSC 102-2218-E-035-009).

Notes

Yu-Cheng Chang, Department of Materials Science and Engineering, Feng Chia University, No. 100, Wenhwa Rd., Seatwen, Taichung 40724, Taiwan. E-Mail: ychang0127@gmail.com; FAX. 886-4-24510014; TEL. 886-4-24517250 Ext.5348

† Electronic Supplementary Information (ESI) available: SEM images of ball-like ZnO nanoplates grown on Si wafer with ZnO seeds layer, and schematic diagram illustrates the processes and substrates to catalyze the degradation of phenol by sunlight. See DOI: 10.1039/b000000x/

References

1. U. Ozgur, Y. I. Alivov, C. Liu, A. Teke, M. A. Reshchikov, S. Dogan, V. Avrutin, S. J. Cho and H. Morkoc, *Journal of Applied Physics*, 2005, **98**, 041301-041103.
2. Z. Fan and J. G. Lu, *Journal of Nanoscience and Nanotechnology*, 2005, **5**, 1561-1573.
3. Z. L. Wang, *Materials Today*, 2004, **7**, 26-33.
4. Y. C. Kong, D. P. Yu, B. Zhang, W. Fang and S. Q. Feng, *Applied Physics Letters*, 2001, **78**, 407-409.
5. Y. Liu, Y. Li and H. Zeng, *Journal of Nanomaterials*, 2013, **2013**, 9.
6. W. Zhong Lin, *Journal of Physics: Conference Series*, 2006, **26**, 1.
7. S. Xu, Z.-H. Li, Q. Wang, L.-J. Cao, T.-M. He and G.-T. Zou, *Journal of Alloys and Compounds*, 2008, **465**, 56-60.
8. M. H. Huang, S. Mao, H. Feick, H. Yan, Y. Wu, H. Kind, E. Weber, R. Russo and P. Yang, *Science*, 2001, **292**, 1897-1899.
9. H. Zhou, M. Wissinger, J. Fallert, R. Hauschild, F. Stelzl, C. Klingshirn and H. Kalt, *Applied Physics Letters*, 2007, **91**, 181112-181113.
10. M.-T. Chen, M.-P. Lu, Y.-J. Wu, J. Song, C.-Y. Lee, M.-Y. Lu, Y.-C. Chang, L.-J. Chou, Z. L. Wang and L.-J. Chen, *Nano Letters*, 2010, **10**, 4387-4393.
11. R. Könenkamp, R. C. Word and M. Godinez, *Nano Letters*, 2005, **5**, 2005-2008.
12. X. D. Wang, C. Neff, E. Graugnard, Y. Ding, J. S. King, L. A. Pranger, R. Tannenbaum, Z. L. Wang and C. J. Summers, *Advanced Materials*, 2005, **17**, 2103-2106.
13. Y.-C. Chang, H.-W. Wu, H.-L. Chen, W.-Y. Wang and L.-J. Chen, *The Journal of Physical Chemistry C*, 2009, **113**, 14778-14782.
14. P. Jae Young, S. Dong Eon and K. Sang Sub, *Nanotechnology*, 2008, **19**, 105503.
15. G. N. Dar, A. Umar, S. A. Zaidi, S. Baskoutas, S. W. Hwang, M. Abaker, A. Al-Hajry and S. A. Al-Sayari, *Talanta*, 2012, **89**, 155-161.
16. P.-C. Chang, Z. Fan, C.-J. Chien, D. Stichtenoth, C. Ronning and J. G. Lu, *Applied Physics Letters*, 2006, **89**, 263102.
17. N. A. Andrey and P. S. Igor, *Journal of Physics D: Applied Physics*, 2010, **43**, 315104.
18. H. Wu, D. Lin, R. Zhang and W. Pan, *Journal of the American Ceramic Society*, 2008, **91**, 656-659.
19. M.-P. Lu, J. Song, M.-Y. Lu, M.-T. Chen, Y. Gao, L.-J. Chen and Z. L. Wang, *Nano Letters*, 2009, **9**, 1223-1227.
20. Z. L. Wang and J. Song, *Science*, 2006, **312**, 242-246.
21. P. Fei, P.-H. Yeh, J. Zhou, S. Xu, Y. Gao, J. Song, Y. Gu, Y. Huang and Z. L. Wang, *Nano Letters*, 2009, **9**, 3435-3439.
22. X. Zhang, X. Huang, C. Li and H. Jiang, *Advanced Materials*, 2013, **25**, 4093-4096.
23. Y.-J. Lee, D. S. Ruby, D. W. Peters, B. B. McKenzie and J. W. P. Hsu, *Nano Letters*, 2008, **8**, 1501-1505.
24. P.-C. Chang, Z. Fan, D. Wang, W.-Y. Tseng, W.-A. Chiou, J. Hong and J. G. Lu, *Chemistry of Materials*, 2004, **16**, 5133-5137.
25. S. T. Tan, B. J. Chen, X. W. Sun, W. J. Fan, H. S. Kwok, X. H. Zhang and S. J. Chua, *Journal of Applied Physics*, 2005, **98**, 013505.
26. W. Z. Xu, Z. Z. Ye, Y. J. Zeng, L. P. Zhu, B. H. Zhao, L. Jiang, J. G. Lu, H. P. He and S. B. Zhang, *Applied Physics Letters*, 2006, **88**, 173506.
27. L. Wang, X. Zhang, S. Zhao, G. Zhou, Y. Zhou and J. Qi, *Applied Physics Letters*, 2005, **86**, 024108.
28. D. C. Look, D. C. Reynolds, C. W. Litton, R. L. Jones, D. B. Eason and G. Cantwell, *Applied Physics Letters*, 2002, **81**, 1830-1832.
29. X. W. Sun and H. S. Kwok, *Journal of Applied Physics*, 1999, **86**, 408-411.
30. E. M. Kaidashev, M. Lorenz, H. Von Wenckstern, A. Rahm, H. C. Semmelhack, K. H. Han, G. Benndorf, C. Bundesmann, H. Hochmuth and M. Grundmann, *Applied Physics Letters*, 2003, **82**, 3901-3903.

31. W. L. Hughes and Z. L. Wang, *Journal of the American Chemical Society*, 2004, **126**, 6703-6709.
32. S. Xu and Z. Wang, *Nano Res.*, 2011, **4**, 1013-1098.
33. L. E. Greene, B. D. Yuhas, M. Law, D. Zitoun and P. Yang, *Inorganic Chemistry*, 2006, **45**, 7535-7543.
34. Z. R. Tian, J. A. Voigt, J. Liu, B. McKenzie, M. J. McDermott, M. A. Rodriguez, H. Konishi and H. Xu, *Nat Mater*, 2003, **2**, 821-826.
35. Y. Tak and K. Yong, *The Journal of Physical Chemistry B*, 2005, **109**, 19263-19269.
36. L. Vayssieres, *Advanced Materials*, 2003, **15**, 464-466.
37. J. Bae, J. B. Han, X.-M. Zhang, M. Wei, X. Duan, Y. Zhang and Z. L. Wang, *The Journal of Physical Chemistry C*, 2009, **113**, 10379-10383.
38. Z. Yunyan and M. Jin, *Nanotechnology*, 2007, **18**, 075606.
39. R. Vinod, P. Sajan, A. Sreekumar Rajappan, T. Carmen Martinez, M.-S. Vicente and M. J. Bushiri, *Journal of Physics D: Applied Physics*, 2012, **45**, 425103.
40. P. Gao, Y. Chen, Y. Wang, Q. Zhang, X. Li and M. Hu, *Chemical Communications*, 2009, 2762-2764.
41. Y. C. Chang and L. J. Chen, *The Journal of Physical Chemistry C*, 2007, **111**, 1268-1272.
42. Y. H. Tong, Y. C. Liu, C. L. Shao and R. X. Mu, *Applied Physics Letters*, 2006, **88**, 123111.
43. N. T. Khoa, S. W. Kim, D. V. Thuan, D.-H. Yoo, E. J. Kim and S. H. Hahn, *CrystEngComm*, 2013.
44. Y. Qiu, W. Chen and S. Yang, *Journal of Materials Chemistry*, 2010, **20**, 1001-1006.
45. G. Amin, M. H. Asif, A. Zainelabdin, S. Zaman, O. Nur and M. Willander, *Journal of Nanomaterials*, 2011, **2011**.
46. Z. Wang, X.-f. Qian, J. Yin and Z.-k. Zhu, *Langmuir*, 2004, **20**, 3441-3448.
47. Z. R. Tian, J. A. Voigt, J. Liu, B. McKenzie and M. J. McDermott, *Journal of the American Chemical Society*, 2002, **124**, 12954-12955.
48. T. Zhang, W. Dong, M. Keeter-Brewer, S. Konar, R. N. Njabon and Z. R. Tian, *Journal of the American Chemical Society*, 2006, **128**, 10960-10968.
49. T. L. Sounart, J. Liu, J. A. Voigt, J. W. P. Hsu, E. D. Spoerke, Z. Tian and Y. B. Jiang, *Advanced Functional Materials*, 2006, **16**, 335-344.
50. Y.-C. Chang, W.-C. Yang, C.-M. Chang, P.-C. Hsu and L.-J. Chen, *Crystal Growth & Design*, 2009, **9**, 3161-3167.
51. L. P. Bauermann, J. Bill and F. Aldinger, *The Journal of Physical Chemistry B*, 2006, **110**, 5182-5185.
52. S. J. Padayatty, A. Katz, Y. Wang, P. Eck, O. Kwon, J.-H. Lee, S. Chen, C. Corpe, A. Dutta, S. K. Dutta and M. Levine, *Journal of the American College of Nutrition*, 2003, **22**, 18-35.
53. L. E. Greene, M. Law, D. H. Tan, M. Montano, J. Goldberger, G. Somorjai and P. Yang, *Nano Letters*, 2005, **5**, 1231-1236.
54. H. Zeng, X. Xu, Y. Bando, U. K. Gautam, T. Zhai, X. Fang, B. Liu and D. Golberg, *Advanced Functional Materials*, 2009, **19**, 3165-3172.
55. C.-W. Chen, K.-H. Chen, C.-H. Shen, A. Ganguly, L.-C. Chen, J.-J. Wu, H.-I. Wen and W.-F. Pong, *Applied Physics Letters*, 2006, **88**, 241905
56. F. Lu, W. Cai and Y. Zhang, *Advanced Functional Materials*, 2008, **18**, 1047-1056.
57. X. Cao, H. Zeng, M. Wang, X. Xu, M. Fang, S. Ji and L. Zhang, *The Journal of Physical Chemistry C*, 2008, **112**, 5267-5270.
58. S. Senapati, S. K. Srivastava and S. B. Singh, *Nanoscale*, 2012, **4**, 6604-6612.
59. S. Ahmed, M. Rasul, W. Martens, R. Brown and M. Hashib, *Water, Air, and Soil Pollution*, 2011, **215**, 3-29.
60. Y. Liu, N. Zhao and W. Gao, *RSC Advances*, 2013, **3**, 21666-21674.

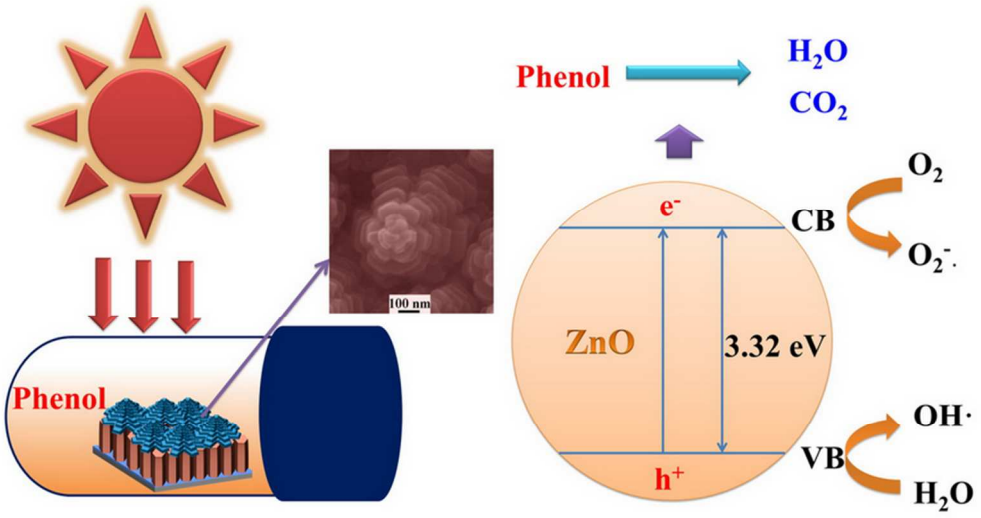

ZnO nanopinecone arrays exhibit a much better photocatalytic property for the photodegradation of phenol in sunlight.
74x39mm (300 x 300 DPI)